IET Journals
The Institution of Engineering and Technology

Exact closed-form capacity and outage probability of physical layer security in $\kappa - \mu$ shadowed fading channels

ISSN 1751-8644
doi: 0000000000
www.ietdl.org

Hussien Al-Hmood[1*], *Hamed Al-Raweshidy*[2]

[1] *Electrical and Electronic Engineering (EEE) Department, College of Engineering, University of Thi-Qar, Nassiriyah, Thi-Qar, Iraq*
[2] *Electrical and Computer Engineering (ECE) Department, College of Engineering, Design and Physical Sciences, Brunel University London, Uxbridge, UB8 3PH, UK*
* *E-mail: Hussien.Al-Hmood@brunel.ac.uk, Hussien.Al-Hmood@eng.utq.edu.iq*

Abstract: In this paper, the secrecy performance of physical layer when both the main and wiretap channels undergo $\kappa - \mu$ shadowed fading conditions is analysed. In particular, the average secrecy capacity (ASC), secure outage probability (SOP), the lower bound of SOP (SOP^L), and the probability of strictly positive secrecy capacity (SPSC) are derived by using the classic Wyner's wiretap model. Two different scenarios for the fading parameters, namely, μ and m, which represent the real extension of the number of the multipath clusters and the shadowing index, respectively, have been studied. These parameters are chosen first as arbitrary numbers, thus the performance metrics are given in exact closed-form in terms of the extended generalized bivariate Fox's H-function (EGBFHF) that has been widely implemented in the open literature using various software packages. In the second scenario, both the fading parameters are assumed to be integer numbers to obtain the derived results in simple exact closed-form mathematically tractable expressions in terms of some analytic functions. The numerical results of this analysis are verified via the Monte Carlo simulations.

1 Introduction

Wyner developed the information-theoretic notion of perfect secrecy that was introduced by Shannon via proposing the wiretap channel in addition to the main channel [1]. Accordingly, the performance analysis of the physical layer security over fading channels was given a special attention in the open literature. For example, the probability of strictly positive secrecy capacity (SPSC), the secure outage probability (SOP), and the average secrecy capacity (ASC) when the wireless channels undergo the additive white Gaussian noise (AWGN) and Rayleigh fading channel were derived in [2] and [3], respectively. The authors in [4] studied the SPSC when both the main and wiretap channels subject to Rician fading conditions. The SOP and SPSC over Rician/Nakagami-m and Nakagami-m/Rician fading scenarios were provided in [5]. The SPSC and the ASC of the Weibull fading channel were introduced in [6] and [7], respectively. The closed-form expression of the SPSC when the main and the wiretap channels experience a log-normal fading was presented in [8].

Recently, many efforts were devoted to analysing the secrecy performance of the physical layer over different generalized fading channels which give results closer to the practical measurement than the traditional distributions. For instance, the closed-form expressions for the SPSC and the lower bound of SOP (SOP^L) over generalised Gamma fading model were derived by using the classic Wyner's wiretap model [9]. The authors in [10] analysed the SPSC and SOP^L over $\kappa - \mu$ fading that is used to model the line-of-sight (LoS) communication scenario where the parameters κ and μ denote the ratio between the powers of the dominant and the scattered waves components and the number of multipath clusters, respectively. In [11] and [12], the SPSC and the ASC were, respectively, utilised to studying the secrecy performance over $\alpha - \mu$ fading condition, which was proposed to represent the non-homogeneous environment of wireless channel where α indicates the non-linearity index. The scenario of main/wiretap channels undergo $\alpha - \mu/\kappa - \mu$ fading conditions was investigated in [13] and [14] to study the security of the physical layer via deriving the SPSC, the SOP, and the SOP^L and the asymptotic expression of the SOP at high signal-to-noise ratio (SNR) and the SOP^L, respectively. In both works, the performance metrics were expressed in terms of the Meijer's G-function and infinite series.

The wireless channel may subject to the shadowing effect which is part of fading that can not be ignored. Hence, several works were dedicated to analysing the security of physical layer over composite multipath/shadowed fading channels. The generalised-K (K_G) fading model, which is composite of Nakagami-m/Gamma distributions, was employed for both the mai and the wiretap channels of the classic Wyner's framework in [15] and [16]. In the former, the ASC, the SOP, and the SPSC were expressed in terms of the extended generalized bivariate Meijer's G-function (EGBMGF) whereas a mixture Gamma (MG) distribution was used in the latter to approximate with high accuracy the same performance metrics. The work in [17] was also used the MG fading channel model via expressing the probability density function (PDF) and cumulative distribution function (CDF) in terms of a single variable Fox's H-function (FHF).

The physical layer security over the so-called $\kappa - \mu$ shadowed fading channel that has been suggested as a composite of $\kappa - \mu$ and Nakagami-m distributions was investigated by several efforts. The authors in [18] studied the physical layer security over $\kappa - \mu$ shadowed fading by employing the incomplete moment generating function (IMGF) for integer values of the fading parameters. But, the derived results were given in terms of the partial derivative of the upper IMGF which would lead to provide the performance metrics with double infinite series. This is because the upper IMGF of the $\kappa - \mu$ shadowed fading model was expressed in terms of the confluent Lauricella hypergeometric Φ_2 function. On contrary, in [19], the SOP, SPSC, and ASC for $\kappa - \mu$ shadowed fading scenarios were presented in terms of an integral form. The analysis in [20] was also based on using the $\kappa - \mu$ shadowed fading channels to deriving the SPSC and SOP^L of the physical layer. However, the provided expressions were approximated and included the EGBMGF as well as double infinite series that do not converge easily and steadily. Therefore, the authors were used the Gamma distribution to approximate the expressions of the aforementioned performance metrics in

simple closed-from formats. In [21], the SOP and SPSC for single-input multiple-output over independent and identically distributed (i.i.d.) $\kappa-\mu$ shadowed fading channels with integer values of μ were given in terms of double infinite summations. Although the single variable FHF is recently utilised in [22] as a unified framework to analysing the physical layer security over several channels such as $\alpha-\mu$, it cannot be applied for $\kappa-\mu$ shadowed fading condition. This is because impossibility of expressing both the PDF and the CDF of $\kappa-\mu$ shadowed fading in terms of the univariate FHF.

Motivated by the above, this work is dedicated to providing another formats of the secrecy performance metrics of the physical layer over $\kappa-\mu$ shadowed fading channel via using two different scenarios of the fading parameters.

The main contributions of this work that fill the gaps of [18], [19], [20], and [21] are listed as follows:

- We derive exact closed-from expression of the confluent Lauricella hypergeometric Φ_2 function in terms of the extended generalized bivariate Fox's H-function (EGBFHF). This function has been widely implemented in the open literature using MATLAB and MATHEMATICA software packages.
- Capitalising on the above, we comprehensively analyse the secrecy performance of the physical layer over $\kappa-\mu$ shadowed fading channel model via deriving novel exact closed-form expressions of the ASC, SOP, SOP^L, and SPSC for arbitrary and integer numbers of the fading parameters. However, in [20] and [21], the SOP^L and SPSC were only given in terms of double infinite series. Although the ASC was derived in both [18] and [19], the provided expressions were presented in an integral form and infinite series, respectively.
- Unlike the SOP^L and SPSC of [20] and [21] that were included double infinite series when the fading parameters are arbitrary values, our derived expressions are exact closed-form.
- We study the secrecy performance of the physical layer over $\kappa-\mu$ shadowed fading model by assuming μ and the shadowing severity index are integer numbers. Consequently, the ASC, SOP, SOP^L, and SPSC are obtained in simple exact closed-form mathematically tractable analytic expressions. In addition, they provide good insights into the behaviour of the systems at different values of the fading parameters. Although this scenario was investigated in [18] and [19] for the ASC and the SOP, the derived results were given in terms of double infinite series as well as non-analytic function. It is remarkable that the case of the fading parameters are integer valued was not presented in [20] and [21].
- In contrast to [21] in which the Gamma distribution was utilised to providing the SOP^L and SPSC in approximate closed-form, our derived results are given in exact expressions via supposing the values of the fading parameters are integer numbers.

Organization: Section 2 is divided into two subsections. In Subsection 2.1, the system model is described whereas the formats of the PDF and CDF of $\kappa-\mu$ shadowed fading are given in Subsection 2.2. The ASC, the SOP, the SOP^L, and the SPSC for general and integer values of μ and shadowing parameter are derived in Sections 3, 4, 5, and 6, respectively. Section 7 performs the simulations and numerical results. Finally, conclusions are presented in Section 8.

2 System and Channel Models

2.1 System Model

The model defined by Wyner in [1] consists of three different nodes of wireless communications. The legitimate user communicates with the intended receiver which are named Alice and Bob, respectively, in the presence of an eavesdropper (Eve). In this paper, it is supposed that the main (Alice-Bob) and wiretap (Alice-Eve) channels that are independent undergo quasi-static $\kappa-\mu$ shadowed fading channels. Moreover, all nodes are equipped with a single antenna and the channel state information (CSI) for the main and the wiretap channels is known by the Bob and the Eve, respectively. When the transmitter (Alice) sends the signal $s(n)$, the received signals $r_i(n)$ at the receivers (Bob and Eve) is expressed as [20]

$$r_i(n)=h_i(n)s(n)+w_i(n). \tag{1}$$

where $i\in\{D,E\}$, D, and E stand for Bob, and eavesdropper, respectively. In addition, $h_i(n)$ and $w_i(n)$ are the $\kappa-\mu$ shadowed fading channel and the additive white Gaussian noise that has zero mean and fixed variance, respectively.

2.2 The PDF and CDF of $\kappa-\mu$ Shadowed Fading

The PDF of the instantaneous SNR γ_i, $f_{\gamma_i}(\gamma_i)$, in $\kappa-\mu$ shadowed fading model is given by [23, eq. (4)]

$$f_{\gamma_i}(\gamma_i)=\Theta_i\gamma_i^{\mu_i-1}e^{-\mathcal{A}_i\gamma_i}{}_1F_1(m_i;\mu_i;\mathcal{B}_i\gamma_i). \tag{2}$$

where $\mathcal{A}_i=\frac{\mu_i(1+\kappa_i)}{\bar{\gamma}_i}$, $\Theta_i=\frac{m_i^{m_i}\mathcal{A}_i^{\mu_i}}{\Gamma(\mu_i)(\mu_i\kappa_i+m_i)^{m_i}}$, $\mathcal{B}_i=\frac{\mu_i\kappa_i\mathcal{A}_i}{(\mu_i\kappa_i+m_i)}$, $\bar{\gamma}_i$ is the average SNR, m_i is the shadowing severity index, and ${}_1F_1(.;.;.)$ is the confluent hypergeometric function defined in [24, eq. (9.14.1)].

The CDF of the $\kappa-\mu$ shadowed fading channel is expressed as [23, eq. (6)]

$$F_{\gamma_i}(\gamma_i)=\frac{\Theta_i}{\mu_i}\gamma_i^{\mu_i}\Phi_2\big(\mu_i-m_i,m_i;\mu_i+1;-\mathcal{A}_i\gamma_i,-\mathcal{C}_i\gamma_i\big). \tag{3}$$

where $\mathcal{C}_i=\frac{m_i}{\mu_i\kappa_i+m_i}\mathcal{A}_i$, $\Phi_2(.,.;.;.,.)$ is the bivariate confluent hypergeometric function [22, eq. (9.261.2)].

When both μ and m are integer numbers, i.e., μ and $m\in\mathbb{Z}^+$, the PDF and the CDF are, respectively, given by [25, eqs. (12) and (13)]

$$f_{\gamma_i}(\gamma_i)=\sum_{j_i=0}^{M_i}\Lambda_{j_i}\frac{\gamma_i^{\psi_{j_i}-1}}{\Omega_{j_i}^{\psi_{j_i}}(\psi_{j_i}-1)!}e^{-\frac{\gamma_i}{\Omega_{j_i}}}. \tag{4}$$

and

$$F_{\gamma_i}(\gamma_i)=1-\sum_{j_i=0}^{M_i}\Lambda_{j_i}e^{-\frac{\gamma_i}{\Omega_{j_i}}}\sum_{r_i=0}^{\psi_{j_i}-1}\frac{1}{r_i!}\left(\frac{\gamma_i}{\Omega_{j_i}}\right)^{r_i}. \tag{5}$$

where M_i, Λ_{j_i}, ψ_{j_i}, and Ω_{j_i} are given in Table I that is given on the next page.

3 Average Secrecy Capacity

The ASC is defined as the average of the secrecy capacity C_s over the instantaneous SNR, γ, of the main and the eavesdropper channels. Mathematically, the ASC can be calculated by $\bar{C}_s=I_1+I_2-I_3$ [16, eq. (6)] where I_1, I_2, and I_3 are expressed as

$$I_1=\int_0^\infty \ln(1+\gamma_D)f_D(\gamma_D)F_E(\gamma_D)d\gamma_D \tag{6}$$

$$I_2=\int_0^\infty \ln(1+\gamma_E)f_E(\gamma_E)F_D(\gamma_E)d\gamma_E \tag{7}$$

$$I_3=\int_0^\infty \ln(1+\gamma_E)f_E(\gamma_E)d\gamma_E \tag{8}$$

Theorem 1. *For arbitrary values of μ and m, I_1, I_2, and I_3 are respectively given by (9), (10), and (11) as shown on the next page. In these expressions, $\Gamma(a)=\int_0^\infty x^{a-1}e^{-x}dx$ and $H_{p,q;c,d;\ldots;d_n,c_n}^{s,r:a,b;\ldots;a_n,b_n}[.]$ are the incomplete Gamma function and the EGBFHF defined in [26, A.1], respectively. It can be noticed that the EGBFHF is not yet implemented in popular software packages such as MATLAB and MATHEMATICA. Therefore, several codes*

Table 1 Parameter Values for the PDF and the CDF of the $\kappa-\mu$ Shadowed Fading with Integer μ AND m [25].

Case	Parameters
$\mu_i > m_i$	$M_i = \mu_i$ $\Lambda_{j_i} = \begin{cases} 0, & j_i = 0 \\ (-1)^{m_i}\binom{m_i+j_i-2}{j_i-1}\left[\frac{\mathcal{C}_i}{\mathcal{A}_i}\right]^{m_i}\left[\frac{\mathcal{B}_i}{\mathcal{A}_i}\right]^{-m_i-j_i+1}, & 0 < j_i \leqslant \mu_i - m_i \\ (-1)^{j_i-\mu_i+m_i-1}\binom{j_i-2}{j_i-\mu_i+m_i-1}\left[\frac{\mathcal{C}_i}{\mathcal{A}_i}\right]^{j_i-\mu_i+m_i-1}\left[\frac{\mathcal{B}_i}{\mathcal{A}_i}\right]^{-j_i+1}, & \mu_i - m_i < j_i \leqslant \mu_i \end{cases}$ $\psi_{j_i} = \begin{cases} \mu_i - m_i - j_i + 1, & 0 \leqslant j_i \leqslant \mu_i - m_i \\ \mu_i - j_i + 1, & \mu_i - m_i < j_i \leqslant \mu_i \end{cases}$ $\Omega_{j_i} = \begin{cases} \frac{1}{\mathcal{A}_i}, & 0 \leqslant j_i \leqslant \mu_i - m_i \\ \frac{1}{\mathcal{C}_i}, & \mu_i - m_i < j_i \leqslant \mu_i \end{cases}$
$\mu_i \leqslant m_i$	$M_i = m_i - \mu_i$ $\Lambda_{j_i} = \binom{m_i-\mu_i}{j_i}\left[\frac{\mathcal{C}_i}{\mathcal{A}_i}\right]^{j_i}\left[\frac{\mathcal{B}_i}{\mathcal{A}_i}\right]^{m_i-\mu_i-j_i}$ $\psi_{j_i} = m_i - j_i$ $\Omega_{j_i} = \frac{1}{\mathcal{C}_{j_i}}$

have been written to evaluate this function using various software packages such as [12] and [27].

Proof: See Appendix A for the proof. □

Remark 1. *When both μ and m are integer numbers, (6), (7), and (8) can be yielded in simple exact closed-form expressions as shown at the bottom of this page in (12), (13), and (14), respectively.*

$$I_3^{\text{int}} = \sum_{j_E=0}^{M_E} \Lambda_{j_E} e^{\mathcal{C}_{j_E}} \sum_{k=1}^{\psi_{j_E}} \frac{\Gamma(k-\psi_{j_E}, \mathcal{C}_{j_E})}{\Omega_{j_E}^{\psi_{j_E}-k}} \tag{14}$$

where $\Gamma(a,b) = \int_b^\infty x^{a-1}e^{-x}dx$ is the upper incomplete Gamma function [20, eq. (3.351.2)].

Proof: See Appendix B for the proof. □

$$I_1 = \frac{\Theta_D\Theta_E}{(\mathcal{A}_D-\mathcal{B}_D)^{\mu_D-\mu_E}} \frac{\Gamma(\mu_D)\Gamma(\mu_E)}{\Gamma(\mu_D-m_D)\Gamma(\mu_E-m_E)\Gamma(m_E)} \times H_{1,1:2,2;1,2;1,2;1,1;1,1}^{0,1:1,2;1,1;1,1;1,1;1,1}\left[\frac{1}{\mathcal{A}_D-\mathcal{B}_D}, \frac{\mathcal{B}_D}{\mathcal{A}_D-\mathcal{B}_D}, \frac{\mathcal{A}_E}{\mathcal{A}_D-\mathcal{B}_D}, \frac{\mathcal{C}_E}{\mathcal{A}_D-\mathcal{B}_D}\middle|\begin{matrix}(1-\mu_D+m_D;1,1,1,1)\\(-\mu_E;0,0,1,1)\end{matrix}\middle|\begin{matrix}(1,1),(1,1)\\(1,1),(0,1)\end{matrix}\middle| \begin{matrix}(1-\mu_D+m_D,1)\\(0,1),(1-\mu_D,1)\end{matrix}\middle|\begin{matrix}(1-\mu_E+m_E,1)\\(0,1)\end{matrix}\middle|\begin{matrix}(1-m_E,1)\\(0,1)\end{matrix}\right] \tag{9}$$

$$I_2 = \frac{\Theta_E\Theta_D}{(\mathcal{A}_E-\mathcal{B}_E)^{\mu_E-\mu_D}} \frac{\Gamma(\mu_E)\Gamma(\mu_D)}{\Gamma(\mu_E-m_E)\Gamma(\mu_D-m_D)\Gamma(m_D)} \times H_{1,1:2,2;1,2;1,1;1,1;1,1}^{0,1:1,2;1,1;1,1;1,1;1,1}\left[\frac{1}{\mathcal{A}_E-\mathcal{B}_E}, \frac{\mathcal{B}_E}{\mathcal{A}_E-\mathcal{B}_E}, \frac{\mathcal{A}_D}{\mathcal{A}_E-\mathcal{B}_E}, \frac{\mathcal{C}_D}{\mathcal{A}_E-\mathcal{B}_E}\middle|\begin{matrix}(1-\mu_E+m_E;1,1,1,1)\\(-\mu_D;0,0,1,1)\end{matrix}\middle|\begin{matrix}(1,1),(1,1)\\(1,1),(0,1)\end{matrix}\middle| \begin{matrix}(1-\mu_E+m_E,1)\\(0,1),(1-\mu_E,1)\end{matrix}\middle|\begin{matrix}(1-\mu_D+m_D,1)\\(0,1)\end{matrix}\middle|\begin{matrix}(1-m_D,1)\\(0,1)\end{matrix}\right] \tag{10}$$

$$I_3 = \Theta_E \frac{\Gamma(\mu_E)}{\Gamma(\mu_E-m_E)} H_{1,0:2,2;1,2}^{0,1:1,2;1,1,2}\left[\frac{1}{\mathcal{A}_E-\mathcal{B}_E}, \frac{\mathcal{B}_E}{\mathcal{A}_E-\mathcal{B}_E}\middle|\begin{matrix}(1-\mu_E,1)\\-\end{matrix}\middle|\begin{matrix}(1,1),(1,1)\\(1,1),(0,1)\end{matrix}\middle|\begin{matrix}(1-\mu_E+m_E,1)\\(0,1),(1-\mu_E,1)\end{matrix}\right] \tag{11}$$

$$I_1^{\text{int}} = \sum_{j_D=0}^{M_D} \Lambda_{j_D}\left[e^{\mathcal{C}_{j_D}} \sum_{k=1}^{\psi_{j_D}} \frac{\Gamma(k-\psi_{j_D}, \mathcal{C}_{j_D})}{\Omega_{j_D}^{\psi_{j_D}-k}} - \sum_{j_E=0}^{M_E} \Lambda_{j_E} e^{\mathcal{C}_{j_D}+\mathcal{C}_{j_E}} \sum_{r_E=0}^{\psi_{j_E}-1} \frac{(\psi_{j_D})_{r_E}}{r_E!} \sum_{l=1}^{\psi_{j_D}+r_E} \frac{\Gamma(l-\psi_{j_D}-r_E, \mathcal{C}_{j_D}+\mathcal{C}_{j_E})}{\Omega_{j_D}^{\psi_{j_D}-l}\Omega_{j_E}^{r_E-l}(\Omega^{\psi_{j_D}}+\Omega^{\psi_{j_E}})^l}\right] \tag{12}$$

$$I_2^{\text{int}} = \sum_{j_E=0}^{M_E} \Lambda_{j_E}\left[e^{\mathcal{C}_{j_E}} \sum_{k=1}^{\psi_{j_E}} \frac{\Gamma(k-\psi_{j_E}, \mathcal{C}_{j_E})}{\Omega_{j_E}^{\psi_{j_E}-k}} - \sum_{j_D=0}^{M_D} \Lambda_{j_D} e^{\mathcal{C}_{j_E}+\mathcal{C}_{j_D}} \sum_{r_D=0}^{\psi_{j_D}-1} \frac{(\psi_{j_E})_{r_D}}{r_D!} \sum_{l=1}^{\psi_{j_E}+r_D} \frac{\Gamma(l-\psi_{j_E}-r_D, \mathcal{C}_{j_E}+\mathcal{C}_{j_D})}{\Omega_{j_E}^{\psi_{j_E}-l}\Omega_{j_D}^{r_D-l}(\Omega^{\psi_{j_E}}+\Omega^{\psi_{j_D}})^l}\right] \tag{13}$$

It can be observed that the ASC over $\kappa-\mu$ shadowed fading channel has not been presented in exact closed-form expression in the previous works. Consequently, to the authors' best knowledge, the expressions in (9)-(14) are novel.

4 Secure Outage Probability

The SOP is defined as the probability of falling the instantaneous secrecy capacity, C_s, of the system below the target secrecy threshold, R_s. According to [9, eq. (4)], the SOP can be computed by

$$\text{SOP} = \int_0^\infty F_D(\theta\gamma_E + \theta - 1) f_E(\gamma_E) d\gamma_E \tag{15}$$

where $\theta = \exp(R_s) \geq 1$, i.e., $R_s \geq 0$.

Theorem 2. *For arbitrary and integer values of the fading parameters, the SOP and SOP^{int} are given in (16) and (17), respectively, at the bottom of this page. In (17), $\binom{b}{a} \triangleq \frac{b!}{(b-a)!}$ denotes the binomial coefficient.*

Proof: See Appendix C for the proof. □

One can see that (16) and (17) are new because they have not been derived in the open technical literature in exact closed-from.

5 Lower Bound of SoP

According to [6], the SOP^L can be obtained from (15) by inserting $\gamma_E \to \infty$. Hence, the SOP^L can be calculated by

$$\begin{aligned}\text{SOP}^L &= \int_0^\infty F_D(\theta\gamma_E) f_E(\gamma_E) d\gamma_E \\ &\leq \text{SOP}\end{aligned} \tag{18}$$

Theorem 3. *: The SOP^L for arbitrary numbers of μ and m, the SOP^L can be expressed in terms of the multivariate FHF as given in (19). Moreover, when μ and $m \in \mathbb{N}^+$, the SOP$^L_{int}$ can be obtained in simple exact closed-from expression as in (20).*

Proof: See Appendix D for the proof. □

$$\begin{aligned}\text{SOP}^L_{\text{int}} = 1 - \sum_{j_E=0}^{M_E} \frac{\Lambda_{j_E}}{\Omega_{j_E}^{\psi_{j_E}} (\psi_{j_E}-1)!} \sum_{j_D=0}^{M_D} \Lambda_{j_D} \\ \sum_{r_D=0}^{\psi_{j_D}-1} \frac{\theta^{r_D}}{\Omega_{j_D}^{\psi_{j_D}} r_D!} \frac{\Gamma(\psi_{j_E}+r_D)}{\left(\frac{\theta}{\Omega_{j_D}} + \frac{1}{\Omega_{j_E}}\right)^{\psi_{j_E}+r_D}}\end{aligned} \tag{20}$$

6 Probability of Strictly Positive Secrecy Capacity

The SPSC that is defined as the probability of the instantaneous secrecy capacity, C_s, is greater than zero can be evaluated by [9, eq. (12)]

$$\text{SPSC} = 1 - \text{SOP}^L \quad \text{for} \quad \theta = 1 \tag{21}$$

Accordingly, the SPSC for arbitrary and integer values of fading parameters can be deduced from (19) and (20), respectively, after using $\theta = 1$ and plugging the results in (21).

7 Numerical and Simulation Results

In this section, the numerical results of this work are verified via Monte Carlo simulations with 10^7 iterations. The parameters of main and wiretap channels are assumed to be independent and non-identically distributed random variables. In all figures, the markers represents the numerical results, whereas the solid lines explain the simulations. Furthermore, all the secrecy performance metrics are plotted versus $\bar{\gamma}_D$ and the ratio $\lambda = \bar{\gamma}_D/\bar{\gamma}_E$ for various values of μ_D and m_D and $\bar{\gamma}_D$, respectively.

Figs. 1 illustrates the ASC versus λ for (μ_D, m_D) = $(0.5, 0.5), (2, 0.5), (2, 4)$, $\kappa_D = \kappa_E = 1$, $\mu_E = 0.5$, $m_E = 1$, and $\bar{\gamma}_E = 5$ dB. From this figure, one can see that the value of the ASC becomes better when μ_D or/and m_D increase. This is because the high values of μ and m imply a large number of multipath clusters and less shadowing impact at the Bob, respectively. For instance, at $m_D = 0.5$ and $\lambda = 20$ (fixed), the ASC for $\mu_D = 2.5$ is nearly 17%

$$\begin{aligned}\text{SOP} = \Theta_D\Theta_E \frac{(\theta-1)^{\mu_D+\mu_E}}{\theta^{\mu_E}} \frac{\Gamma(\mu_E)}{\Gamma(\mu_E-m_E)\Gamma(\mu_D-m_D)\Gamma(m_D)} \\ \times H^{1,1:1,0;1,1;1,1;1,1}_{2,2:0,1;1,2;1,1;1,1}\left[\frac{(\theta-1)}{\theta}(\mathcal{A}_E-\mathcal{B}_E), \frac{(\theta-1)}{\theta}\mathcal{B}_E, (\theta-1)\mathcal{A}_D, (\theta-1)\mathcal{C}_D \middle| \begin{matrix}(1-\mu_E;1,1,0,0),(-\mu_D;0,0,1,1)\\(-\mu_D;0,0,1,1),(-\mu_D-\mu_E;1,1,1,1)\end{matrix}\right. \\ \left. - \begin{matrix}(1-\mu_E+m_E,1)\\(0,1),(1-\mu_E,1)\end{matrix}\middle| \begin{matrix}(1-\mu_D+m_D,1)\\(0,1)\end{matrix}\middle| \begin{matrix}(1-m_D,1)\\(0,1)\end{matrix}\right]\end{aligned} \tag{16}$$

$$\text{SOP}^{\text{int}} = 1 - \sum_{j_D=0}^{M_D} \Lambda_{j_D} e^{-\frac{\theta-1}{\Omega_{j_D}}} \sum_{r_D=0}^{\psi_{j_D}-1} \frac{1}{\Omega_{j_D}^{r_D} r_D!} \sum_{j_E=0}^{M_E} \frac{\Lambda_{j_E}}{\Omega_{j_E}^{\psi_{j_E}} (\psi_{j_E}-1)!} \sum_{k=0}^{r_D} \binom{r_D}{k} \frac{\theta^k \Gamma(k+\psi_{j_E})}{(\theta-1)^{k-r_D}\left(\frac{\theta}{\Omega_{j_D}} + \frac{1}{\Omega_{j_E}}\right)^{k+\psi_{j_E}}} \tag{17}$$

$$\begin{aligned}\text{SOP}^L = \Theta_D\Theta_E \frac{\theta^{\mu_D}}{(\mathcal{A}_E-\mathcal{B}_E)^{\mu_D+\mu_E}} \frac{\Gamma(\mu_E)}{\Gamma(\mu_E-m_E)\Gamma(\mu_D-m_D)\Gamma(m_D)} \\ \times H^{0,1:1,1;1,1;1,1}_{1,1:1,2;1,1;1,1}\left[\frac{\mathcal{B}_E}{(\mathcal{A}_E-\mathcal{B}_E)}, \frac{\theta\mathcal{A}_D}{(\mathcal{A}_E-\mathcal{B}_E)}, \frac{\theta\mathcal{C}_D}{(\mathcal{A}_E-\mathcal{B}_E)} \middle| \begin{matrix}(1-\mu_E-\mu_D;1,1,1)\\(-\mu_D;0,1,1)\end{matrix}\middle| \begin{matrix}(1-\mu_E+m_E,1)\\(0,1),(1-\mu_E,1)\end{matrix}\middle| \begin{matrix}(1-\mu_D+m_D,1)\\(0,1)\end{matrix}\middle| \begin{matrix}(1-m_D,1)\\(0,1)\end{matrix}\right]\end{aligned} \tag{19}$$

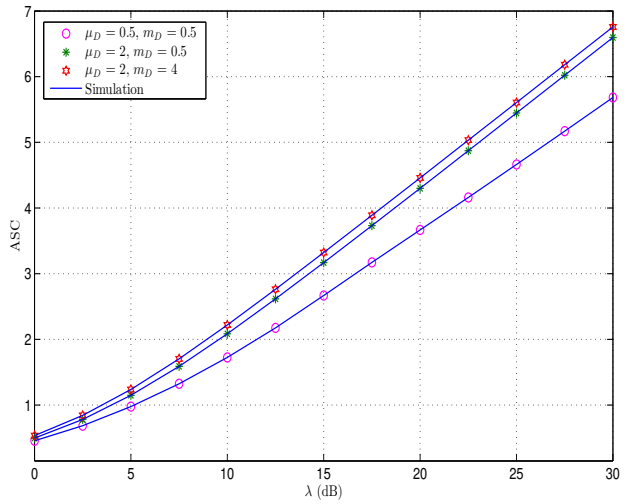

Fig. 1: ASC versus λ for different values of μ_D and m_D, $\kappa_D = \kappa_E = 1$, $\mu_E = 0.5$, $m_E = 1$, and $\bar{\gamma}_E = 5$ dB

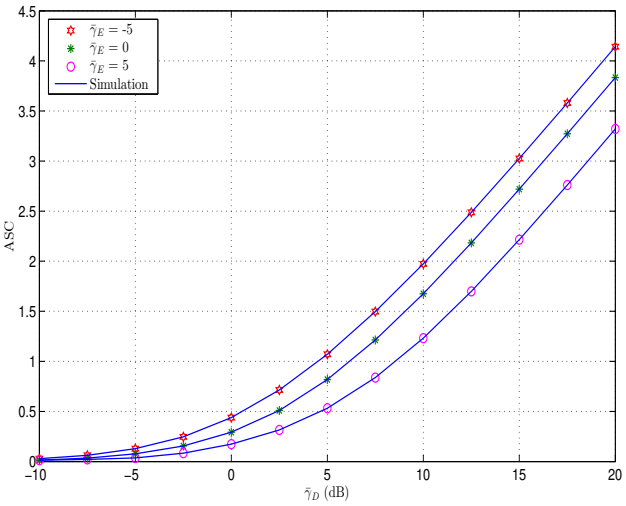

Fig. 2: ASC versus $\bar{\gamma}_D$ for different values of $\bar{\gamma}_E$, $\kappa_D = \kappa_E = 1$, $\mu_D = 2.5$, $m_D = 1.5$, $\mu_E = 0.5$, and $m_E = 1$

higher than $\mu_D = 0.5$. In the same context, when $\mu_D = 2$ and m_D changes from 0.5 to 4, the ASC is increased by roughly 4%.

Fig. 2 shows the ASC versus $\bar{\gamma}_D$ for $\bar{\gamma}_E = -5, 0$, and 5 dB, $\kappa_D = \kappa_E = 1$, $\mu_D = 2.5$, $m_D = 1.5$, $\mu_E = 0.5$, and $m_E = 1$. In this figure, it can be observed that the increasing in $\bar{\gamma}_D$ leads to enhancing the security performance. On the other side, the ASC improves when $\bar{\gamma}_E$ decreases. This refers to the deterioration of the eavesdropper's channel. For example, when $\bar{\gamma}_D = 10$ dB (fixed), the values of the ASC for $\bar{\gamma}_E = -5$ dB and $\bar{\gamma}_E = 0$ dB are approximately 1.974 and 1.675, respectively.

Figs. 3 and 4 demonstrate both the SOP and SOP^L versus λ and $\bar{\gamma}_D$, respectively, for $R_s = 1$ and the same simulation parameters of Figs. 1 and 2. As expected, the the SOP and SOP^L reduce with the increasing in the fading parameters of the main channel i.e., μ_D and m_D and for the same reasons that are mentioned previously. Moreover, under the same conditions, the difference between the SOP and SOP^L becomes large when $\bar{\gamma}_E$ increases. This is because the total SNR of the SOP^L is higher than that of the SOP. For example, in Fig. 3, at $\lambda = 15$ (fixed), the SOP and SOP^L for the (μ_D, m_D) = (2, 4) are less by nearly 40.4% and 40.2%, respectively, than (μ_D, m_D) = (2, 0.5). The provided results for the SOP in Figs. 2 and 3 are affirmed by the SOP^L in the same figures. This confirmation comes from all results of the SOP^L in the these figures are less than their corresponding scenarios of the SOP and this satisfies the second equal of (18).

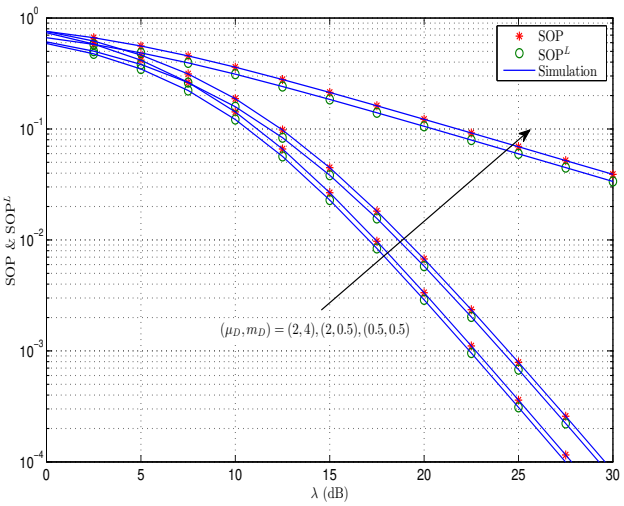

Fig. 3: SOP and SOP^L versus λ for different values of μ_D and m_D, $\kappa_D = \kappa_E = 1$, $\mu_E = 0.5$, $m_E = 1$, $\bar{\gamma}_E = 5$ dB, and $R_s = 1$

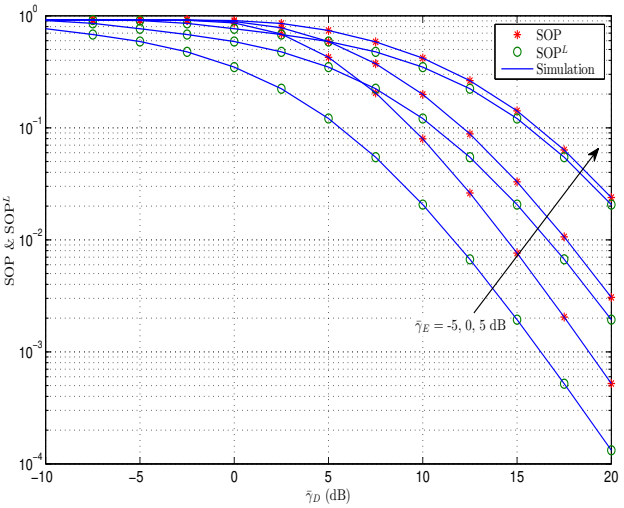

Fig. 4: SOP and SOP^L versus $\bar{\gamma}_D$ for different values of $\bar{\gamma}_E$, $\kappa_D = \kappa_E = 1$, $\mu_D = 2.5$, $m_D = 1.5$, $\mu_E = 0.5$, $m_E = 1$, and $R_s = 1$

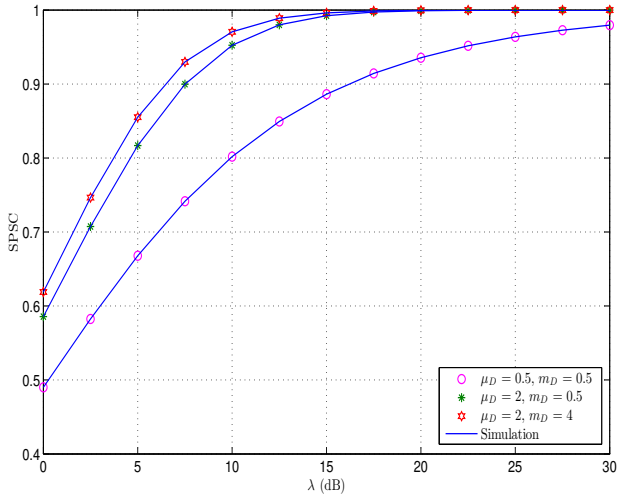

Fig. 5: SPSC versus λ for different values of μ_D and m_D, $\kappa_D = \kappa_E = 1$, $\mu_E = 0.5$, $m_E = 1$, and $\bar{\gamma}_E = 5$ dB

Figs. 5 and 6 explain the SPSC versus λ and $\bar{\gamma}_D$, respectively. Again, the provided curves in these figures confirm the results of Figs. 1-4.

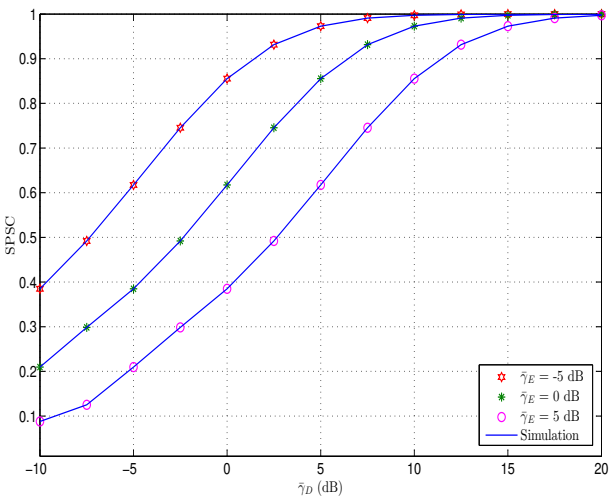

Fig. 6: SPSC versus $\bar{\gamma}_D$ for different values of $\bar{\gamma}_E$, $\kappa_D = \kappa_E = 1$, $\mu_D = 2.5$, $m_D = 1.5$, $\mu_E = 0.5$, and $m_E = 1$

From all figures, it is clear that the performance improves when the ratio λ increases. This refers to the high $\bar{\gamma}_D$ in comparison with the $\bar{\gamma}_E$ which would lead to make the Alice-Bob channel better than the Alice-Eve channel. More importantly, the numerical results and Monte Carlo simulations are in perfect match for any provided scenario.

8 Conclusions

This paper was dedicated to studying the secrecy behaviour of the physical layer over $\kappa - \mu$ shadowed fading channels. Unlike previous works that are used the same channel model, the secrecy performance metrics, namely, the ASC, the SOP, the SOP^L, and the SPSC, were derived by assuming two different scenarios of the fading parameters. In the first scenario, the derived results were expressed in exact closed-form in terms of the EGBFHF for arbitrary values of μ and m. On the other side, the second scenario provided analytic exact mathematically tractable closed-form expressions in terms of simple functions via assuming the fading parameters are integer numbers. From the given results, an enhancement in the values of the ASC, the SOP, the SOP^L, and the SPSC can be observed when μ_D or/and m_D increase and $\bar{\gamma}_E$ decreases. Accordingly, the results of this work can be employed to studying the behaviour of the physical layer security over a variety of fading channels with simple exact closed-form expressions and integer fading parameters. The case of the imperfect CSI over $\kappa - \mu$ shadowed fading channels can be also taken into consideration in our next work.

9 References

1 Wyner, A.D.:'The wire-tap channel', *Bell Syst. Tech. J.*, Oct. 1975, **54**, (8), pp. 1355-1387

2 Barros, J., and Rodrigues, M.R.D.:'Secrecy capacity of wireless channels', *Proc. IEEE Int. Symp. Inf. Theory (ISIT)*, Seattle, WA, July 2006, pp. 356-360

3 Bloch, M., Barros, J., Rodrigues, M.R.D., and McLaughlin, S.W.:'Wireless information-theoretic security', *IEEE Trans. Inf. Theory*, June 2008, **54**, (6), pp. 2515-2534

4 Liu, X.:'Probability of strictly positive secrecy capacity of the Rician-Rician fading channel', *IEEE Wireless Commun. Lett.*, Feb. 2013, **2**, (1), pp. 50-53

5 Iwata, S., Ohtsuki, T., and Kam, P.Y.: 'Performance analysis of physical layer security over Rician/Nakagami-m fading channels', *Proc. IEEE Veh. Technol. Conf. (VTC Spring)*, Sydney, NSW, June 2017, pp. 1-6

6 Liu, X.: 'Probability of strictly positive secrecy capacity of the Weibull fading channel', *Proc. IEEE Global Commun. Conf. (GLOBECOM)*, Atlanta, GA, June 2013, pp. 659-664

7 Liu, X.:'Average secrecy capacity of the Weibull fading channel', *Proc. IEEE Annual Consumer Commun. Net. Conf. (CCNC)*, Las Vegas, NV, 2016, pp. 841-844

8 Liu, X.:'Secrecy capacity of wireless links subject to log-normal fading', *Proc. IEEE Conf. Commun. Net. (CCN)*, China, Kun Ming, Jan. 2012, pp. 167-172

9 Lei, H., Gao, C., Guo, Y., and Pan, G.:'On physical layer security over generalized gamma fading channels', *IEEE Commun. Lett.*, July 2015, **19**, (7), pp. 1257-1260

10 Bhargav, N., Cotton, S.L., and Simmons, D.E.:'Secrecy capacity analysis over $\kappa - \mu$ fading channels: Theory and applications', *IEEE Trans. Commun.*, July 2016, **64**, (7), pp. 3011-3024

11 Kong, L., Tran, H., and Kaddoum, G.:'Performance analysis of physical layer security over $\alpha - \mu$ fading channel', *Electron. Lett.*, Jan. 2016, **52**, (1), pp. 45-47

12 Lei, H., Zhang, H., Ansari, I.S., Pan, G., Alomair, B., and Alouini, M.S.:'Secrecy capacity analysis over $\alpha - \mu$ fading channels', *IEEE Commun. Lett.*, June 2017, **21**, (6), pp. 1445-1448

13 Bhargav, N., and Cotton, S.L.:'Secrecy capacity analysis for $\alpha - \mu/\kappa - \mu$ and $\kappa - \mu/\alpha - \mu$ fading scenarios', *Proc. IEEE Pers., Indoor, and Mob. Radio Commun. (PIMRC)*, Valencia, 2016, pp. 1-6

14 Moualeu, J.M., and Hamounda, W.:'Performance analysis of secure communications over $\alpha - \mu/\kappa - \mu$ fading channels', *Proc. IEEE Int. Conf. Computer Engineering and Systems (ICCES)*, Cairo, Egypt, Dec. 2017, pp. 473-478

15 Lei, H., Zhang, H., Ansari, I.S., Gao., C., Guo, Y., Pan, G., and Qaraqe, K.A.:'Physical layer security over generalized-K fading channels', *IET Commun.*, July 2016, **10**, (16), pp. 2233-2237

16 Lei, H., Zhang, H., Ansari, I.S., Gao., C., Guo, Y., Pan, G., and Qaraqe, K.A.:'Performance analysis of physical layer security over generalized-K fading channels using a mixture gamma distribution', *IEEE Commun. Lett.*, Feb. 2016, **20**, (2), pp. 408-411

17 Kong, L., and Kaddoum, G.:'Secrecy characteristics with assistance of mixture gamma distribution', *IEEE Commun. Lett.*, March 2019, **00**, (0), pp. 1-1

18 Lopez-Martinez, F.J., Romero-Jerez, J.M., and Paris, J.F.:'On the calculation of the incomplete MGF with applications to wireless communications', *IEEE Trans. Commun.*, Jan. 2017, **65**, (1), pp. 458-469

19 Nunes, M.M., and Dias, U.S.: 'On the physical layer security under $\kappa - \mu$ shadowed fading channels with diversity approaches', *Proc. Symp. Telecommun. Processing of Sig. (BSTPS)*, Brazil Sept. 2017, pp. 373-377

20 Sun, J., Li, X., Huang, M., Ding, Y., Jin, J., and Pan, G.: 'Performance analysis of physical layer security over $\kappa - \mu$ shadowed fading channels', *IET Commun.*, May 2018, **12**, (8), pp. 970 - 975

21 Srinivasan, M., and Kalyani, S.:'Secrecy capacity of $\kappa - \mu$ shadowed fading channels', *IEEE Commun. Lett.*, Aug. 2018, **22**, (8), pp. 1728-1731

22 Kong, L., Kaddoum, G., and Chergui, H.:'On physical layer security over Fox's H-function wiretap fading channels', *IEEE Trans. Veh. Technol.*, March 2019, **00**, (0), pp. 1-1

23 Paris, J.F.:'Statistical characterization of $\kappa - \mu$ shadowed fading', *IEEE Trans. Veh. Technol.*, Feb. 2014, **63**, (2), pp. 518-526

24 Gradshteyn, I.S., and Ryzhik, I.M.:', *Table of Integrals, Series and Products*, 7th edition. Academic Press Inc., 2007

25 Lopez-Martinez, F.J., Paris, J.F., and Romero-Jerez, J.M.:'The $\kappa - \mu$ shadowed fading model with integer fading parameters', *IEEE Trans. Veh. Technol.*, Sept. 2017, **66**, (9), pp. 7653-7662

26 Mathai, A.M., Saxena, R.K., and Haubold, H.J.:*The H-function: theory and applications*, Springer Science & Business Media, 2009

27 Alhennawi, H.R., Ayadi, M.M.H.E., Ismail, M.H., and Mourad, H.A.M.:'Closed-form exact and asymptotic expressions for the symbol error rate and capacity of the H-function fading channel', *IEEE Trans. Veh. Technol.*, Apr. 2016, **65**, (4), pp. 1957-1974

28 Srivastava, H.M., and Manocha, H.L.:*A treatise on generating functions*, Wiley, New York, 1984

29 Adamchik, V.S., and Marichev, O.I.:'The algorithm for calculating integrals of hypergeometric type functions and its realization in REDUCE system', *Proc. IEEE ISSAC*, Tokyo, Japan, Aug. 1990, pp. 212-224

30 Jung, J., *et al.*:'Capacity and error probability analysis of diversity reception schemes over generalized-K fading channels using a mixture gamma distribution', *IEEE Trans. Wireless Commun.*, Sept. 2014, **13**, (9), pp. 4721-4730

Appendix A

Proof of Theorem 1

Substituting (2) and (3) in (6), we have

$$I_1 = \frac{\Theta_D \Theta_E}{\mu_E} \int_0^\infty \ln(1+\gamma_D) \gamma_D^{\mu_D + \mu_E - 1} e^{-\mathcal{A}_D \gamma_D} \times {}_1F_1(m_D; \mu_D; \mathcal{B}_D \gamma_D) \times \Phi_2\big(\mu_E - m_E, m_E; \mu_E + 1; -\mathcal{A}_E \gamma_D, -\mathcal{C}_E \gamma_D\big) d\gamma_D \quad (22)$$

To compute the integral in (22) in exact closed-form, we express $\ln(.)$ and the hypergeometric functions in terms of the Meijer G-function. However, the argument of ${}_1F_1(.;.;.)$ should be negative to be expressed in terms of the single variable FHF and the integral converges. To achieve that, the following properties [28, eq. (1.3.7)],

[26, eq. (1.130)], and [29, eq. (11)] are used in (22)

$$ {}_1F_1(a;b;x) = e^x {}_1F_1(b-a;b;-x) \tag{23}$$

$$ {}_1F_1(a;b;-x) = \frac{\Gamma(b)}{\Gamma(a)} H_{1,2}^{1,1}\left[x\middle|\begin{matrix}(1-a,1)\\(0,1),(1-b,1)\end{matrix}\right] \tag{24}$$

$$ \ln(1+x) = H_{2,2}^{1,2}\left[x\middle|\begin{matrix}(1,1),(1,1)\\(1,1),(0,1)\end{matrix}\right] \tag{25}$$

To write the confluent Lauricella hypergeometric function $\Phi_2(.)$ in (22) in terms of the FHF, we use the following identity [28, 1.ii, pp. 259]

$$\Phi_2(a_1,a_2;b;-x_1t,-x_2t) = \frac{1}{t^{b-1}}\mathcal{L}^{-1}\left\{\frac{\Gamma(b)}{s^b}\left(1+\frac{x_1}{s}\right)^{-a_1}\left(1+\frac{x_2}{s}\right)^{-a_2};s,t\right\} \tag{26}$$

where $\Re(b)>0, \Re(s)>0$, and $\{a_1,a_2\}\in\mathbb{R}$ and $\mathcal{L}^{-1}(.)$ stands for the inverse Laplace transform.

The following property is given in [26, eq. (1.43)]

$$(1+x)^{-y} = \frac{1}{\Gamma(y)} H_{1,1}^{1,1}\left[x\middle|\begin{matrix}(1-y,1)\\(0,1)\end{matrix}\right] \tag{27}$$

With the aid of (27) and using the definition of FHF that is presented in [26, eq. (1.2)], the inverse Laplace transform of (26) can be rewritten as

$$\mathcal{L}^{-1}\left\{\frac{\Gamma(b)}{s^b}\left(1+\frac{x_1}{s}\right)^{-a_1}\left(1+\frac{x_2}{s}\right)^{-a_2};s,t\right\} = \frac{\Gamma(b)}{\Gamma(a_1)\Gamma(a_2)} \frac{1}{(2\pi j)^2}\int_{\mathcal{R}_1}\int_{\mathcal{R}_2}\Gamma(r_1)\Gamma(a_1-r_1)\Gamma(r_2)\Gamma(a_2-r_2)x_1^{-r_1}x_2^{-r_2} \mathcal{L}^{-1}\Big\{s^{r_1+r_2-b};s,t\Big\}dr_1dr_2 \tag{28}$$

The inverse Laplace transform in (28) can be calculated as follows

$$\mathcal{L}^{-1}\Big\{s^{r_1+r_2-b};s,t\Big\} = \frac{t^{b-r_1-r_2-1}}{\Gamma(b-r_1-r_2)} \tag{29}$$

Substituting (29) into (28) to yield

$$\mathcal{L}^{-1}\left\{\frac{\Gamma(b)}{s^b}\left(1+\frac{x_1}{s}\right)^{-a_1}\left(1+\frac{x_2}{s}\right)^{-a_2};s,t\right\} = \frac{\Gamma(b)}{\Gamma(a_1)\Gamma(a_2)} t^{b-1}\frac{1}{(2\pi j)^2}\int_{\mathcal{R}_1}\int_{\mathcal{R}_2}\frac{\Gamma(r_1)\Gamma(a_1-r_1)\Gamma(r_2)\Gamma(a_2-r_2)}{\Gamma(b-r_1-r_2)} (xt)_1^{-r_1}(xt)_2^{-r_2}dr_1dr_2 \tag{30}$$

Employing the definition of the bivariate FHF that is given in [26, eq. (2.56)] for (30) along with (26), we have

$$\Phi_2\big(a_1,a_2;b;-x_1t,-x_2t\big) = \frac{\Gamma(b)}{\Gamma(a_1)\Gamma(a_2)} \times H_{0,1:1,1;1,1}^{0,0:1,1;1,1}\left[x_1t,x_2t\middle|\begin{matrix}-\\(1-b,1)\end{matrix}\middle|\begin{matrix}(1-a_1,1)\\(0,1)\end{matrix}\middle|\begin{matrix}(1-a_2,1)\\(0,1)\end{matrix}\right] \tag{31}$$

where $H_{p,q:c,d;d_n,c_n}^{s,r:a,b;a_n,b_n}[.]$ is the bivariate FHF.

After inserting (23), (24), (25) and (31) in (22) and utilising the definition of the FHF, we obtain (32) that is shown at the bottom of this page in terms of the multiple closed contours $\mathcal{R}_i$ in the complex r_i-plane for $i\in\{1,2,3,4\}$.

With the help of [26, eq. (3.381.4)], the inner integral, J_1, of (32) can be be computed in exact closed-form as

$$J_1 = \int_0^\infty \gamma_D^{\mu_D+\mu_E-r_1-r_2-r_3-r_4-1}e^{-(\mathcal{A}_D-\mathcal{B}_D)\gamma_D}d\gamma_D = \frac{\Gamma(\mu_D+\mu_E-r_1-r_2-r_3-r_4)}{(\mathcal{A}_D-\mathcal{B}_D)^{\mu_D+\mu_E-r_1-r_2-r_3-r_4}} \tag{33}$$

Plugging (33) in (32) and using [26, eq. (A.1)], the proof is completed for (9).

It can be observed that (10) can be calculated by (9) after replacing the symbols D and E with E and D, respectively.

Substituting (2) in (8), we have

$$I_3 = \Theta_E\int_0^\infty \ln(1+\gamma_E)\gamma_E^{\mu_E-1}e^{-\mathcal{A}_E\gamma_E} \times {}_1F_1(m_E;\mu_E;\mathcal{B}_E\gamma_E)d\gamma_E \tag{34}$$

Using (23), (24), (25) for (34), this yields

$$I_3 = \Theta_E\frac{\Gamma(\mu_E)}{\Gamma(\mu_E-m_E)}\int_0^\infty \gamma_E^{\mu_E-1}e^{-(\mathcal{A}_E-\mathcal{B}_E)\gamma_E} H_{2,2}^{1,2}\left[\gamma_E\middle|\begin{matrix}(1,1),(1,1)\\(1,1),(0,1)\end{matrix}\right]H_{1,2}^{1,1}\left[\mathcal{B}_E\gamma_E\middle|\begin{matrix}(1-\mu_E+m_E,1)\\(0,1),(1-\mu_E,1)\end{matrix}\right]d\gamma_E \tag{35}$$

Following the same steps in (32) and (33), (35) can be evaluated in exact closed-form expression as provided in (11) which completes the proof.

$$I_1 = \frac{\Theta_D\Theta_E}{\mu_E}\frac{\Gamma(\mu_D)\Gamma(1+\mu_E)}{\Gamma(\mu_D-m_D)\Gamma(\mu_E-m_E)\Gamma(m_E)} \frac{1}{(2\pi j)^4}\int_{\mathcal{R}_1}\int_{\mathcal{R}_2}\int_{\mathcal{R}_3}\int_{\mathcal{R}_4}\frac{\Gamma(1+r_1)\Gamma(-r_1)\Gamma(-r_1)\Gamma(r_2)\Gamma(\mu_D-m_D-r_2)}{\Gamma(1-r_1)\Gamma(\mu_D-r_2)}\frac{\Gamma(r_3)\Gamma(\mu_E-m_E-r_3)\Gamma(r_4)\Gamma(m_E-r_4)}{\Gamma(1-\mu_E-r_3-r_4)} \mathcal{B}_D^{-r_2}\mathcal{A}_E^{-r_3}\mathcal{C}_E^{-r_4}\underbrace{\int_0^\infty \gamma_D^{\mu_D+\mu_E-r_1-r_2-r_3-r_4-1}e^{-(\mathcal{A}_D-\mathcal{B}_D)\gamma_D}d\gamma_D}_{J_1}dr_1dr_2dr_3dr_4 \tag{32}$$

Appendix B

Proof of Remark 1

Inserting (4) and (5) in (6) and performing some mathematical simplifications, this yields

$$I_1^{int} = \sum_{j_D=0}^{M_D} \frac{\Lambda_{j_D}}{\Omega_{j_D}^{\psi_{j_D}}(\psi_{j_D}-1)!} \Bigg[\int_0^{\infty} \ln(1+\gamma_D)\gamma_D^{\psi_{j_D}-1} e^{-\frac{\gamma_D}{\Omega_{j_D}}} d\gamma_D - \sum_{j_E=0}^{M_E} \Lambda_{j_E} \sum_{r_E=0}^{\psi_{j_E}-1} \frac{1}{\Omega_{j_E}^{r_E} r_E!} \times \int_0^{\infty} \ln(1+\gamma_D)\gamma_D^{\psi_{j_D}+r_E-1} e^{-\left(\frac{1}{\Omega_{j_D}}+\frac{1}{\Omega_{j_E}}\right)\gamma_D} d\gamma_D \Bigg] \quad (36)$$

Employing [30, eq. (47)] to calculate both the integrals of (36) in simple exact closed-form expressions as given in (12) and this completes the proof.

Using D and E instead of E and D, respectively, in (12), the result is I_2^{int} that is given in (13).

Plugging (4) in (8), this yields

$$I_3^{int} = \sum_{j_E=0}^{M_E} \frac{\Lambda_{j_E}}{\Omega_{j_E}^{\psi_{j_E}}(\psi_{j_E}-1)!} \times \int_0^{\infty} \ln(1+\gamma_E)\gamma_E^{\psi_{j_E}-1} e^{-\frac{\gamma_E}{\Omega_{j_E}}} d\gamma_E \quad (37)$$

Likewise, [30, eq. (47)] is utilised to express (37) in exact closed-form as given in (14) which completes the proof.

Appendix C

Proof of Theorem 2

Inserting (2) and (3) in (15) and using (23), the result is

$$\text{SOP} = \frac{\Theta_D\Theta_E}{\mu_E} \int_0^{\infty} \gamma_E^{\mu_E-1}(\theta\gamma_E+\theta-1)^{\mu_D} e^{-(\mathcal{A}_E-\mathcal{B}_E)\gamma_E} \times {}_1F_1(\mu_E-m_E;\mu_E;-\mathcal{B}_E\gamma_E) \times \Phi_2\big(\mu_D-m_D,m_D;\mu_D+1;-\mathcal{A}_D(\theta\gamma_E+\theta-1), -\mathcal{C}_D(\theta\gamma_E+\theta-1)\big)d\gamma_E \quad (38)$$

To compute the integral in (38), we recall the identities (23), (24), (31), and [26, eq. (1.39)]. Consequently, the SOP in (38) can be expressed in multiple closed integrals as shown in (39).

Performing some mathematical manipulations and using [24, eq. (3.194.3)] to evaluate J_2 of (39) in exact closed-form as follows

$$J_2 = \theta^{-\mu_E+r_1+r_2}(\theta-1)^{\mu_D+\mu_E-r_1-r_2-r_3-r_4} \times B(\mu_E-r_1-r_2,-\mu_D-\mu_E+r_1+r_2+r_3+r_4) \quad (40)$$

where $B(.,.)$ is the Beta function defined in [28, eq. (1.1.34)].

Invoking the identity $B(x,y)=\frac{\Gamma(x)\Gamma(y)}{\Gamma(x+y)}$ [28, eq. (1.1.47)] for (40) and inserting the result for J_2 in (39), the SOP can be deduced as in (16) and this completes the proof.

When μ and m are integer numbers, the SOP^{int} can be calculated after substituting (4) and (5) into (15) and using the fact that $\int_0^{\infty} f_{\gamma}(\gamma)d\gamma \triangleq 1$. Thus, this yields

$$\text{SOP}^{int} = 1 - \sum_{j_D=0}^{M_D} \Lambda_{j_D} e^{-\frac{\theta-1}{\Omega_{j_D}}} \sum_{r_D=0}^{\psi_{j_D}-1} \frac{1}{\Omega_{j_D}^{r_D} r_D!} \sum_{j_E=0}^{M_E} \frac{\Lambda_{j_E}}{\Omega_{j_E}^{\psi_{j_E}}(\psi_{j_E}-1)!} \times \int_0^{\infty} \gamma_E^{\psi_{j_E}-1}(\theta\gamma_E+\theta-1)^{r_D} e^{-\left(\frac{\theta}{\Omega_{j_D}}+\frac{1}{\Omega_{j_E}}\right)\gamma_E} d\gamma_E \quad (41)$$

Applying some algebraic simplifications and employing the property $(1+a)^b = \sum_{k=0}^{b}\binom{b}{k}a^k$ [24, eq. (1.111)] in (41), we have

$$\text{SOP}^{int} = 1 - \sum_{j_D=0}^{M_D} \Lambda_{j_D} e^{-\frac{\theta-1}{\Omega_{j_D}}} \sum_{r_D=0}^{\psi_{j_D}-1} \frac{1}{\Omega_{j_D}^{r_D} r_D!} \sum_{j_E=0}^{M_E} \frac{\Lambda_{j_E}}{\Omega_{j_E}^{\psi_{j_E}}(\psi_{j_E}-1)!} \sum_{k=0}^{r_D} \binom{r_D}{k} \theta^k (\theta-1)^{r_D-k} \times \int_0^{\infty} \gamma_E^{\psi_{j_E}+k-1} e^{-\left(\frac{\theta}{\Omega_{j_D}}+\frac{1}{\Omega_{j_E}}\right)\gamma_E} d\gamma_E \quad (42)$$

The integral in (42) can be expressed in simple exact closed-form by using [24, eq. (3.381.4)] to yield (17) which completes the proof.

$$\text{SOP} = \frac{\Theta_D\Theta_E}{\mu_D} \frac{\Gamma(\mu_E)\Gamma(1+\mu_D)}{\Gamma(\mu_E-m_E)\Gamma(\mu_D-m_D)\Gamma(m_D)} \frac{1}{(2\pi j)^4} \int_{\mathcal{R}_1}\int_{\mathcal{R}_2}\int_{\mathcal{R}_3}\int_{\mathcal{R}_4} \frac{\Gamma(r_1)\Gamma(r_2)\Gamma(\mu_E-m_E-r_2)}{\Gamma(\mu_E-r_2)} \frac{\Gamma(r_3)\Gamma(\mu_D-m_D-r_3)\Gamma(r_4)\Gamma(m_D-r_4)}{\Gamma(1-\mu_D-r_3-r_4)} (\mathcal{A}_E-\mathcal{B}_E)^{-r_1}\mathcal{B}_E^{-r_2}\mathcal{A}_D^{-r_3}\mathcal{C}_D^{-r_4} \underbrace{\int_0^{\infty} \gamma_E^{\mu_E-r_1-r_2-1}(\theta\gamma_E+\theta-1)^{\mu_D-r_3-r_4} d\gamma_E}_{J_2} dr_1 dr_2 dr_3 dr_4 \quad (39)$$

$$\mathrm{SOP}^{L} = \frac{\theta^{\mu_D}\Theta_D\Theta_E}{\mu_D}\frac{\Gamma(\mu_E)\Gamma(1+\mu_D)}{\Gamma(\mu_E-m_E)\Gamma(\mu_D-m_D)\Gamma(m_D)} \frac{1}{(2\pi j)^3}\int_{\mathcal{R}_1}\int_{\mathcal{R}_2}\int_{\mathcal{R}_3}\frac{\Gamma(r_1)\Gamma(\mu_E-m_E-r_1)}{\Gamma(\mu_E-r_1)}\frac{\Gamma(r_2)\Gamma(\mu_D-m_D-r_2)\Gamma(r_3)\Gamma(m_D-r_3)}{\Gamma(1-\mu_D-r_2-r_3)} \mathcal{B}_E^{-r_1}\mathcal{A}_D^{-r_2}\mathcal{C}_D^{-r_3}\underbrace{\int_0^{\infty}\gamma_E^{\mu_E+\mu_D-r_1-r_2-r_3-1}e^{-(\mathcal{A}_E-\mathcal{B}_E)}d\gamma_E}_{J_3}dr_1dr_2dr_3 \quad (44)$$

Appendix D

Proof of Theorem 3

Inserting (2) and (3) in (18) and recalling the identity (23), this yields

$$\begin{aligned}\mathrm{SOP}^{L} = {} & \frac{\Theta_D\Theta_E}{\mu_E}\theta^{\mu_D} \\ & \int_0^{\infty}\gamma_E^{\mu_E+\mu_D-1}e^{-(\mathcal{A}_E-\mathcal{B}_E)\gamma_E} \\ & {}_1F_1(\mu_E-m_E;\mu_E;-\mathcal{B}_E\gamma_E) \\ & \times\Phi_2\big(\mu_D-m_D,m_D;\mu_D+1;-\mathcal{A}_D\theta\gamma_E,-\mathcal{C}_D\theta\gamma_E\big)d\gamma_E\end{aligned} \quad (43)$$

With the aid of (24) and (31), (43) can be rewritten as in (44) at the top of this page.

The inner integral in (45), J_3, can be evaluated by utilising [24, eq. (3.381.4)] as follows

$$J_3 = \frac{\Gamma(\mu_E+\mu_D-r_1-r_2-r_3)}{(\mathcal{A}_E-\mathcal{B}_E)^{\mu_E+\mu_D-r_1-r_2-r_3}} \quad (45)$$

Plugging (45) in (44) and using the definition of the multivariate FHF, (19) is obtained which completes the proof.

For integer values of the fading parameters, SOP_{int}^{L} can be computed by plugging (4) and (5) in (18) and utilising $\int_0^{\infty}f_{\gamma}(\gamma)d\gamma \triangleq 1$. Accordingly, we have

$$\begin{aligned}\mathrm{SOP}_{int}^{L} = {} & 1-\sum_{j_E=0}^{M_E}\frac{\Lambda_{j_E}}{\Omega_{j_E}^{\psi_{j_E}}(\psi_{j_E}-1)!} \\ & \sum_{j_D=0}^{M_D}\Lambda_{j_D}\sum_{r_D=0}^{\psi_{j_D}-1}\frac{\theta^{r_D}}{\Omega_{j_D}^{\psi_{j_D}}r_D!} \\ & \int_0^{\infty}\gamma_E^{\psi_{j_E}+r_D-1}e^{-\left(\frac{\theta}{\Omega_{j_D}}+\frac{1}{\Omega_{j_E}}\right)\gamma_E}d\gamma_E\end{aligned} \quad (46)$$

With the aid of [24, eq. (3.381.4)], (46) can be calculated in simple exact closed-form expression as provided in (20) and that completes the proof.